Title

A coupled three-dimensional bonded discrete element and lattice Boltzmann method for fluid-solid coupling in cohesive geomaterials

Author 1

- Min Wang, Dr
- Zienkiewicz Centre for Computational Engineering, Swansea University, Swansea, SA 1 8EN, UK
- Rockfield Software Ltd, Swansea, SA1 8AS, UK

Author 2

- Y.T. Feng, Professor
- Zienkiewicz Centre for Computational Engineering, Swansea University, Swansea, SA 1 8EN, UK

Author 3

- G.N. Pande, Professor Emeritus
- Zienkiewicz Centre for Computational Engineering, Swansea University, Swansea, SA 1 8EN, UK

Author 4

- T.T. Zhao, PhD student
- Zienkiewicz Centre for Computational Engineering, Swansea University, Swansea, SA 1 8EN, UK

Abstract

This paper presents a 3D bonded discrete element and lattice Boltzmann method for resolving the fluid-solid interaction involving complicated fluid-particle coupling in geomaterials. In the coupled technique, the solid material is treated as an assembly of bonded and/or granular particles. A bond model accounting for strain softening in normal contact is incorporated into the discrete element method to simulate the mechanical behaviour of geomaterials; whilst, the fluid flow is solved by the lattice Boltzmann method based on kinetic theory and statistical mechanics. To provide a bridge between theory and application, a 3D algorithm of immersed moving boundary scheme was proposed for resolving fluid-particle interaction. To demonstrate the applicability and accuracy of this coupled method, a benchmark called quicksand, in which particles become fluidized under the driving of upward fluid flow, is first carried out. The critical hydraulic gradient obtained from the numerical results matches the theoretical value. Then, numerical investigation of the performance of granular filters generated according to the well-acknowledged design criteria is given. It is found that the proposed 3D technique is promising, and the instantaneous migration of the protected soils can be readily observed. Numerical results prove that the filters which comply with the design criteria can effectively alleviate or eliminate the appearance of particle erosion in dams.

Keywords

Discrete element method; Lattice Boltzmann method; Fluid-particle coupling; Bond model; Immersed moving boundary

List of notation

m is the mass of the particle;

I is the moment of inertia of the particle;

c is a damping coefficient;

a is the acceleration;

$\ddot{\theta}$ is angular acceleration respectively;

F_c is the contact force independent of bond;

T_c is the corresponding torques;

F_f is the resultant hydrodynamic force;

T_f is the torque caused by the hydraulic force;

F_n^b is the normal bond force;

F_t^b is the tangential bond force;

K_n^b is the normal stiffness for the cement;

K_t^b is the tangential stiffness for the cement;

F_{bn} is the critical tensile force;

F_{bt} is the critical shear strength;

δ is the normal overlap;

δ_t is the tangential displacement;

K_{sf} is the stiffness for softening period;

δ_1 is the overlap corresponding to critical bond strength;

δ_2 is the overlap corresponding to bond breakage;

μ is the friction coefficient;

f_i is the fluid density distribution functions;

x is the coordinate;

t is the time;

Δt is time-step increment;

Ω is the collision operator;

τ is the relaxation time;

f_i^{eq} is the equilibrium distribution function;

e_i is the discrete speed of ith component of each node;

v is the macroscopic velocity of each node;

ω_i is the weighting factors;

ρ is the macroscopic fluid density;

η is the kinematic viscosity;

P is the fluid pressure;

C_S is termed the fluid speed of sound;

C is the lattice speed;

h is the lattice spacing;

υ is the kinematic viscosity of the fluid;

B is a weighting function;

ε is the local solid ratio;

V_S is the nodal volume occupied by the solid particle;

V_N is the whole nodal volume;

F_i is the body force term;

U_s is the velocity of the solid node;

u is the velocity of the fluid part at the node;

U_P is the translation velocity;

ω is the angular velocity of the solid particle;

$D_{15(F)}$ is the diameter through which 15% of filter material will pass;

$D_{15(S)}$ is the diameter through which 15% of soil to be protected will pass;

$D_{85(S)}$ is the diameter through which 85% of soil to be protected will pass;

$R_{erosion}$ is the erosion ratio;

N_1 is the numbers of eroded particles;

N is the total number of the base soil;

r_i is the radius of the particle;

G_s is the specific gravity.

1. Introduction

The fluid-solid coupling has been an active research topic in various engineering disciplines (Ladd and Verberg, 2001, Kafui et al., 2002, Zhu et al., 2008, Wu and Guo, 2012). The complexity of the fluid-solid interaction in porous media originates from the microscopic interactions at the grain level, which makes it more challenging. Much progress has been achieved in solving such problems during the past fifty years. One way is to treat the porous medium as a continuum and the macroscopic behaviour is governed by a set of partial differential equations (Li et al., 1990, Zienkiewicz et al., 1999). In this up-bottom approach, the fluid flow and the fluid-solid interaction are governed by the seepage theory which combines the Darcy law and the equation of continuity. Both the fluid and solid can be solved by the continuum-based approach, e.g. finite element method (FEM). The major strength of this approach is its high computational efficiency. Another class is the bottom-up approach, in which the porous medium is treated as an assembly of granular particles (Hakuno and Tarumi, 1988, El Shamy, 2004, Goodarzi et al., 2015). The macroscopic behaviour is obtained by resolving the microscopic/mesoscopic inter-particle forces in discrete element method (DEM). The fluid-solid coupling and fluid flow in pores can be approached by the mesoscopic particle-based methods, such as smoothed particle hydrodynamics (SPH) (Alejandro, 2008) and lattice Boltzmann method (LBM) (Cook et al., 2004, Strack and Cook, 2007, Feng et al., 2007, Feng et al., 2010, Leonardi et al., 2016). In these fluid solvers, the governing equations of fluid flow are algebraic equations rather than differential equations. Compared to LBM, the principal shortcoming of SPH is the tentative and immature treatment of complex boundaries. Due to the obvious advantages, including the Lagrangian characteristics, nature of parallelism and ease of complex boundary treatments, the LBM coupled with DEM is being attracting an increasing interest of researchers from engineering, mechanics and physics. Unlike the continuum-based approaches which assume the porous media as a macro-scale continuum, the coupled DEM-LBM technique is devoted to resolving the fluid-solid coupling at the microscopic grain level. Therefore, the computing cost of this fully particle-based method is rather expensive. The third class is the combination of particle-based DEM and the continuum-based computational fluid method (CFD). In the early DEM-CFD approach (Tsuji et al., 1992), the fluid-particle systems consist of large-sized fluid cells with small-sized particles submerged in them. For an isolated particle in a fluid, the equation to determine the drag resistance force is well established in CFD. However, for a particulate system, the presence of other particles reduces the space for fluid, generates a high fluid velocity gradient and, as a result, yields an increased shear stress on the particle surface. The effect of the presence of other particles can be considered in terms of local porosity (Di Felice, 1994, Kafui et al., 2002). Hu (1996) proposed a direct numerical simulation (DNS) technique, i.e. a fine resolution of CFD for fluid flow, where the fluid field is resolved at a scale comparable with the particle spacing and the particles are treated as discrete moving boundaries. The DEM-CFD is attractive because of its computational convenience. Recent

application of DEM-CFD in geomechanics can be found in references (Zhao, J. D. & Shan, T. 2013, Jing et al., 2015, Zhao et al., 2017). However, the weakness of this method is the treatment of complicated fluid-particle coupling based on a set of semi-empirical equations.

Although great efforts have been made in the past half century, our understanding of certain special coupling problems, such as the initiation and propagation of hydraulic fractures in petroleum engineering, internal soil erosions of granular filters in hydraulic engineering and the liquefaction analysis in geotechnical engineering, are still far from enough. In aforementioned problems, the intractability almost arises from the microscopic fluid-particle interaction. This characteristic makes the micro-scaled technique more fruitful than the continuum-based method, as the former can provide local and detailed response of porous media. Given these reasons, the coupled DEM-LBM emerged as an effective numerical tool, a good complement of the continuum-based methods. This coupled technique treats the porous medium as an assembly of granular particles. In the real geomaterials, the bond or cementation existing between bonded particles is of paramount importance in their macroscopic mechanical characteristics (Delenne et al., 2004, Jiang et al., 2012). The bonded particle method (BPM) (Potyondy and Cundall, 2004), so-called bonded DEM, can simulate the cohesion force between bonded particles through bond models.

The initially proposed bond model is referred as the contact bond model (Itasca Consulting Group Inc, 2002, Potyondy and Cundall, 2004) in Figs. 1 and 2. It approximates the physical behaviour of cohesion as a pair of elastic springs (or a point of glue) with constant normal and shear stiffness acting at the contact point. These two springs have specified shear and tensile strength. It is unable to reproduce some complicated behaviour of porous media, thus more advanced bond models are required (Potyondy and Cundall, 2004, Potyondy, 2007). Delenne et al. (2004) proposed a bond model where rolling contact was considered. The treatment of normal and tangential contact forces is the same as the contact bond model. The rolling resistance is similar to tangential component in the contact bond model. When moment of force reaches a critical value, the rolling resistance is then removed (Jiang et al. 2006 & 2012). For other advanced bond models, readers can refer to the references (Kazerani et al., 2010, Obermayr et al., 2013, Wang, 2016).

Recently, a two-dimensional bonded particle and lattice Boltzmann method (BPLBM) has been proposed and well demonstrated (Wang at al., 2016, Wang at al., 2017a). This work aims to develop a three-dimensional computational framework for BPLBM, which couples the bonded particle method and the lattice Boltzmann method, for resolving the fluid-solid coupling in geomechanics. Currently, brittle failure bond models are utilised in most simulations of cohesive geomaterials. For geomaterials, the sudden loss of energy is unrealistic in the brittle failure bond model (Kazerani at al., 2010). In most of DEM simulations in geomechanics, the particle size adopted is up-scaled, hence one particle can be treated as a cluster which can be envisioned as an element in FEM. The macroscopic stress-strain relation is supposed to apply. Therefore, to alleviate the rate of energy dissipation during bond breakage, the normal bond

force model with softening effect is adopted in this work. Furthermore, a novel 3D algorithm of immersed moving boundary (IMB) scheme is proposed to resolve fluid-particle interaction. It includes efficient calculation of nodal solid ratio and identification of fluid and solid boundary nodes. The remainder of this paper is organized as follows. In section 2, the theory and general computational procedures of BPM and the formulations of bond models are illustrated firstly, which is followed by a brief elaboration of the lattice Boltzmann method. Next, the coupling algorithm of the immersed moving boundary scheme is presented in more detail in section 3. To quantitatively validate the accuracy of BPLBM, a benchmark called quicksand, in which particles become fluidized under the driving of upward fluid flow, is first given. Then, numerical examples of the transport of fine particles within granular filters in dams are investigated and validated by well-acknowledged design criteria in section 4. Finally, a brief conclusion and potential future work are given in section 5.

2. Computational Methodology

In this coupled method, the solid material is treated as an assembly of bonded and/or granular particles and the macroscopic behaviour of the solid is the comprehensive reflection of the inter-particle interactions. The bond model is utilised to handle the cohesive force between bonded particles, and the treatment of the contact between granular particles is the same as that in DEM. In the meantime, the fluid flow is solved using the lattice Boltzmann method, and the fluid-solid interactions are resolved through the immersed moving boundary (IMB) scheme (Noble and Torczynski, 1998) which is commonly used in the coupled DEM-LBM.

2.1 Bonded particle method

It has been well understood that the bonds existing between adjacent particles can resist both traction and shear forces. It will break due to excessive tension and/or shear forces (Delenne et al., 2004, Jiang et al., 2012). Nowadays BPM is being extensively used for simulating construction materials i.e. soil, rock and concrete.

The principal problems in BPM are the calculation of contact forces and the contact detection. The processing of contact forces will be introduced in the following section. As there has been considerable research on the contact detection algorithm, detailed discussion of this part will be skipped and it can be found in the literatures (Feng and Owen, 2002, Munjiza, 2004). Given the efficiency in terms of CPU and memory, we used the no binary search (NBS) (Munjiza, 2004) contact detection algorithm for dense-packed samples in our in-house code BPLBM3D.

The motion of a particle is governed by Newton's second law

$$ma + cv = F_c + F_f + mg \tag{1}$$

$$I\ddot{\theta} = T_c + T_f \tag{2}$$

where m and I are respectively the mass and the moment of inertia of the particle; *c* is a damping coefficient; a and $\ddot{\theta}$ are the acceleration and angular acceleration respectively; F_c and T_c are, respectively, contact forces and the corresponding torques, F_f and T_f are the hydrodynamic forces and the corresponding torques.

In BPM, there are two interactions between solid particles: the particle-particle contact existing between granular particles and the cohesion between bonded particles. As the treatment of particle-particle interactions is the same as that in DEM and can be found in our previous work (Wang at al., 2016, Wang at al., 2017a), only the introduction of the treatment of cohesion, which is simulated by bond models, will be given in this section.

2.1.1 Bond models

Currently, brittle failure bond models are utilised in most simulations of cohesive geomaterials. For soils the bond is rather soft compared to rock bond. Even for rock, the sudden loss of energy is unrealistic in the brittle failure bond model (Kazerani at al., 2010). To alleviate the rate of energy dissipation during bond breakage, a normal bond force model with softening effect is adopted (see Fig. 3). In the tangential direction, a history dependent Coulomb friction model is used. They can be described as follows

Normal component:

$$F_n^b = \begin{cases} K_n^b \delta & \delta >= \delta_1 \\ K_n^b \delta_1 + K_{sf}(\delta - \delta_1) & \delta_2 < \delta < \delta_1 \\ 0 & \delta < \delta_2 \end{cases} \tag{3}$$

Tangential component:

$$F_t^b = -\frac{\dot{\delta}_t}{\left|\dot{\delta}_t\right|} \begin{cases} K_t^b \left|\delta_t\right|; & \left|K_t^b \delta_t\right| \le \mu F_n^b \\ \mu F_n^b; & \left|K_t^b \delta_t\right| > \mu F_n^b \end{cases} \tag{4}$$

where K_{sf} , δ_1 and δ_2 are the stiffness for softening period, overlap corresponding to critical bond strength and overlap corresponding to bond breakage, respectively. μ is the friction coefficient. δ_t is a vector of tangential displacement, and the over-dot denotes a derivative of time.

2.1.2 General algorithm of BPM

To overcome the difficulty from the theory of BPM to its numerical implementation, a brief computational procedure of the bonded particle method is given in Table 1.

Table 1 Algorithm of BPM

(1) First contact detection and record bonded particle pairs and corresponding initial distances
(2) Install bonds between bonded particles. Relax sample if required.
(3) Global contact detection and calculate overlap between particles in contact
(4) Calculate the particle-particle interaction independent of bonding
(5) Compute cohesion forces for bonded particles and break the bond if its critical value is exceeded
(6) Update the position and velocity of each particle
(7) Set t=t+Δt; go to (3)

In step (1) the first contact detection is performed for building up a bond list of bonded particles. The initial distances between bonded particles are record to obtain a fast relaxation process of the initial particles, when bonded models are applied. Here we propose a reduced-overlap method to ensure a fast relaxation of initial samples. In this method, the deformation of the bond for each pair of bonded particles is subtracted by the initial overlap at each time step. Therefore, the sample should be in equilibrium when bonds are installed.

2.2 Lattice Boltzmann method

The lattice Boltzmann method (Chen et al., 1991) is a class of computational fluid dynamics (CFD) methods. Unlike the traditional CFD methods, which solve the conservation (Navier-Stokes) equations of mass, momentum, and energy numerically. LBM treats the fluid as an assembly of mesoscopic particles. The propagation and interaction of those particles are governed by the lattice Boltzmann equation (see Eq. 5). The primary variables of LBM are fluid density distribution functions instead of pressure and velocity in the conventional CFD. This approach has both Eulerian and Lagrangian nature in the computational point of view. Due to its particulate nature and local dynamics, LBM has several advantages over other conventional CFD methods, especially in dealing with complex boundaries and parallelization of the algorithm.

2.2.1 Bhatnagar-Gross-Krook (BGK) model

Given the computational efficiency and ease in programming, the BGK model is the most adopted. It can be characterised by the following lattice Boltzmann equation:

$$f_i(\boldsymbol{x} + \boldsymbol{e}_i \Delta t, t + \Delta t) - f_i(\boldsymbol{x}, t) = \Omega_i \tag{5}$$

where f_i is the primary variables (so-called fluid density distribution functions); $\boldsymbol{x}, t$ are the coordinate and time, respectively; Δt and Ω_i are the time-step increment and the collision operator.

In the BGK Model, Ω_i is characterised by a relaxation time τ and the equilibrium distribution function $f_i^{eq}(x, t)$

$$\Omega_i = -\frac{\Delta t}{\tau}\left[f_i(\boldsymbol{x}, t) - f_i^{eq}(\boldsymbol{x}, t)\right] \tag{6}$$

The D3Q15 model is the most popular 3D one and it uses a cubic lattice with 15 discrete velocity directions. The fluid particles at each lattice node move to their 14 neighbouring nodes with discrete velocities $\boldsymbol{e_i}$, (i =1-14). A proportion of the particles, with velocity $\boldsymbol{e_0}$, remain at the node. The 15 discrete velocity vectors are given in the following *E* matrix where rows represent directions:

$$E = \begin{bmatrix} 0 & 1 & -1 & 0 & 0 & 0 & 0 & 1 & -1 & 1 & -1 & 1 & -1 & 1 & -1 \\ 0 & 0 & 0 & 1 & -1 & 0 & 0 & 1 & -1 & 1 & -1 & -1 & 1 & -1 & 1 \\ 0 & 0 & 0 & 0 & 0 & 1 & -1 & 1 & -1 & -1 & 1 & 1 & -1 & -1 & 1 \end{bmatrix} \tag{7}$$

The corresponding equilibrium distribution function can be defined as

$$f_i^{eq} = \omega_i \rho(1 + \frac{3}{C^2} e_i \cdot \boldsymbol{v} + \frac{9}{2C^4}(e_i \cdot \boldsymbol{v})^2 - \frac{3}{2C^2} \boldsymbol{v} \cdot \boldsymbol{v}) \qquad (i = 0,...,15) \tag{8}$$

$\boldsymbol{v}$ is the macroscopic velocity of each node; the lattice speed C and weighting factors ω_i are defined as:

$$C = \frac{h}{\Delta t} \tag{9}$$

$$\omega_0 = \frac{2}{9}, \qquad \omega_{1\text{-}6} = \frac{1}{9}, \qquad \omega_{7\text{-}14} = \frac{1}{72} \tag{10}$$

where h is the lattice spacing; Δt is the time step and determined by

$$\Delta t = \frac{h^2}{3\eta}(\tau - 0.5) \tag{11}$$

η is the kinematic viscosity.
The macroscopic fluid density and velocity can be calculated from the distribution functions

$$\rho = \sum_{i=0}^{14} f_i, \qquad \boldsymbol{v} = \sum_{i=1}^{14} f_i e_i / \rho \tag{12}$$

The fluid pressure is given by

$$\Delta p = \Delta \rho C^2 / 3 \tag{13}$$

For more computational details of the implementation of turbulent models and body forces, readers can refer to our previous work (Feng et al., 2007, Feng et al., 2010).

2.3 The fluid-solid coupling

In the 1990s, the LBM was first applied to simulate the fluid-particle coupling problems (Ladd, 1994, Zhang et al., 1999, Ladd and Verberg, 2001). In their method, the modified bounce-back rule (Ladd, 1994, Mansouri et al., 2009, Delenne et al., 2011, Lominé et al., 2013) was used to achieve the no-slip condition at the fluid-particle interface. The particle is divided into a large number of solid nodes by fluid grids. The fluid boundary nodes, exterior to particle surface, and the solid boundary nodes, interior to particle surface, are assumed to be connected by links. The particle boundary is represented by the mid points of links. Apparently, the stepwise lattice representation of the surface of a circular particle is neither accurate nor smooth unless a sufficiently small grid is used. More seriously, when the particle is in motion, its boundary nodes will continually change, which has serious impact in the computed hydrodynamic forces (Feng and Michaelides, 2004, Feng et al., 2007). In order to resolve the aforementioned problem, three approaches have been proposed. The first one is the so-called interpolation-based approach (Filippova and Hänel, 1998, Mei et al., 1999, Mei et al., 2002, Lallemand and Luo, 2003, Yu et al., 2003). It is reported that the interpolation routines used to solve the distribution functions near the curved boundary result in a loss of mass conservation, which reduces the accuracy of the computed momentum transfer at the boundary (Lallemand and Luo, 2003, Kao and Yang, 2008). Later, the interpolation-based approach was improved by treating curved boundaries using an appropriate local refinement grid technique (Kao and Yang, 2008). The second approach is the immersed moving boundary (IMB) scheme proposed by Noble and Torczynski (1998). The hydrodynamic forces at the moving boundary are accomplished by introducing an additional collision term for nodes covered partially or fully by the solid and a weighting function involving the solid fraction within a computational cell. Because of its precise representation of the particle boundary, well computational stability and efficiency, the IMB has been widely used in the coupled DEM-LBM technique where a few thousand particles immersed in the fluid can be considered (Cook et al., 2004, Feng et al., 2007, Strack and Cook, 2007, Feng et al., 2010, Owen et al., 2011, Han and Cundall, 2013, Cui et al., 2014, Leonardi et al., 2016). The immersed boundary (IB) scheme, the last approach, was introduced to the lattice Boltzmann method by Feng and Michaelides (2004) and examined by a couple of researchers (Peng et al., 2006, Shu et al., 2007, Dupuis et al., 2008). It is indicated that the non-slip boundary condition is not fully enforced and the choice of spring constants is arbitrary in the initial IB-LBM. Recently, Shu et al. (2007) proposed an implicit velocity correction based IB-LBM scheme in which the velocity correction should be determined in such a way that the velocity at the boundary interpolated from the corrected velocity field satisfies the non-slip boundary condition. It was then improved in terms of the accuracy of hydrodynamic forces (Wu and Shu, 2009, Wu and Shu, 2010) and computational efficiency (Dash et al., 2014). Considering the

applicability and accuracy (Han and Cundall, 2011, Han and Cundall, 2013), the IMB scheme is adopted for solving the fluid-solid interaction in our program (BPLBM3D).

2.3.1 Formulation of IMB

The immersed moving boundary scheme was proposed by Noble and Torczynski (1998) to overcome fluctuations of hydrodynamic forces calculated by the modified bounce back technique. In this method, the particle is represented by solid nodes, including the solid boundary nodes and interior solid nodes. The fluid nodes near solid boundary nodes are defined as fluid boundary nodes. To facilitate the illustration of the 3D IMB scheme, a cross-section through the centre of a sphere is given in Fig. 4. Four sorts of nodes, solid boundary nodes, interior solid nodes, fluid boundary nodes and normal fluid nodes, are, respectively, marked in red, yellow, green and blue. In order to retain the advantages of LBM, namely the locality of the collision operator and the simple linear streaming operator, an additional collision term, Ω_i^s, for nodes covered partially or fully by the solid is introduced to the standard collision operator of LBM. The modified collision operator for resolving the fluid-solid interaction is given by

$$\Omega_i = -\frac{\Delta t}{\tau}(1-B)[f_i(\boldsymbol{x},t) - f_i^{eq}(\boldsymbol{x},t)] + (1-B)\Delta t F_i + B\Omega_i^S \tag{14}$$

where *B* is a weighting function that depends on the local solid ratio ε, defined as the fraction of the nodal volume.

When *B* is zero, the collision operator is reduced to standard one for fluid. The simplest form of B is that it is equal to the local solid ratio ε.

To eliminate Knudsen layer effects (Noble and Torczynski, 1998) appeared in the simplest form, the following form was proposed and a very good accuracy was obtained.

$$B = \frac{\varepsilon(\tau - 0.5)}{(1-\varepsilon) + (\tau - 0.5)} \tag{15}$$

$$\varepsilon = V_S / V_N \tag{16}$$

V_S is the nodal volume occupied by the solid particle and V_N is the whole nodal volume.

The body force term F_i is determined by the commonly used Guo's method (Guo et al., 2002).

The additional collision term is based on the bounce-rule for non-equilibrium part (Zou and He, 1997) and is given by

$$\Omega_i^S = f_{-i}(\boldsymbol{x},t) - f_i(\boldsymbol{x},t) + f_i^{eq}(\rho, U_S) - f_{-i}^{eq}(\rho, \boldsymbol{u}) \tag{17}$$

where U_S is the velocity of the solid node, and $\boldsymbol{u}$ is the velocity of the fluid part at the node. f_{-i} is used to denote the bounce-back state from f_i.

The velocity of the solid node accounting for the effect of particle rotation is described by

$$U_S = U_P + \omega \times l_P \qquad (l_P = \sqrt{(x - x_P)^2 + (y - y_P)^2 + (z - z_P)^2}) \tag{18}$$

U_P and ω are the translation velocity and angular velocity of the solid particle.

The resultant hydrodynamic force and torque exerted on the solid can be calculated through the momentum theorem, and they are given by

$$F_f = Ch\Big[\sum_n (B_n \sum_i \Omega_i^s e_i)\Big] \tag{19}$$

$$T_f = Ch\Big\{\sum_n \Big[(x - x_P) \times (B_n \sum_i \Omega_i^s e_i)\Big]\Big\} \tag{20}$$

2.3.2 Algorithm of IMB

There are mainly three parts in the implementation algorithm: a) Sorting out fluid boundary and solid boundary nodes; b) Computing the solid ratio ε for boundary nodes associated to the solid particle; c) approaching the interaction between fluid boundary and solid boundary nodes. Among them, the identification of fluid boundary and solid boundary nodes and computation of their solid ratio ε are computationally expansive. Therefore, how to efficiently identify both fluid and solid boundary nodes and compute their solid ratio are of great importance for a particle-fluid coupling simulation involving a number of particles. Although there have been lots of papers on the theory and application of IMB, its implementation is seldom reported (Wang at al., 2017b).

The detailed procedures are given below.

1) Set the centre of sphere as the geometry centre, generate a circumscribed cube of ($\boldsymbol{r} = \boldsymbol{r}_i + h$) side length. h is the lattice size. Loop over all nodes within this cube, record potential fluid boundary and solid boundary nodes lying between a large circle ($\boldsymbol{r} = \boldsymbol{r}_i + h$) and a small circle ($\boldsymbol{r} = \boldsymbol{r}_i - h$).

2) Different to the solid nodal area computed in the 2-D problem, the calculation of the solid nodal volume is very challenging. Hence, the Monte Carlo method is adopted for the calculation of solid fraction within one cubic lattice in this work (see Fig. 5).

Loop over each potential boundary node, a great many points (N_m) are generated randomly within the cube the boundary node under consideration locates.

Then, the total number (N_s) of the random points within the solid particle is determined by the geometry relation. The ratio of the number N_s to the total number N_m is the approximate solid fraction ε. To examine the error of the computed solid fraction, different total number of points (1000, 5000, 10000 and 50000) are generated in one unit cube, respectively. Five samples are generated for each N_m. The random error is given in Fig. 6.

3) Finally, applying the IMB collision operator (Eq. 14) to achieve the coupling between fluid boundary and solid boundary nodes. Meanwhile, the hydrodynamic forces can be calculated by Eqs. 19 and 20.

2.3.3 Two-way coupling procedure

The two-way coupling of BPM and LBM is achieved by the IMB scheme. At each coupling process, the particle geometry, location and movement information is passed to IMB from the solid field; In the meantime, the variables, including density distribution function, velocity and body forces, of the fluid are send to IMB. Once the relaxation of fluid boundary and solid boundary nodes are approached by the collision operator (Eq. 14), then the updated fluid density distribution functions of the node and hydraulic forces applied to the solid particle are respectively transferred to LBM and BPM. The BPM-LBM coupling schematic is given in Fig. 7.

3. Numerical Examples

To evaluate the accuracy and applicability of the proposed coupled method, two test examples are carried out. First, quicksand problems of a single column of spheres with and without bond driven by upward seepage flow are carried out and discussed; Then, a small-scaled granular filter–soil system involving the soil erosion is given to further validate the BPLBM using a well-acknowledged design criterion.

3.1 Quicksand of a single column of spheres

In the first benchmark, a single column of spherical particles of diameter 0.02 m are immersed in water. In the first model (0.02 m × 0.02 m × 0.08 m) shown in Fig. 8, the top three spheres in red are moveable. To make it comparable to model 2, the bottom sphere in blue is fixed. To obtain upward fluid flow, pressure boundary conditions are applied at the bottom and top of the model. The top fluid pressure is 0.0 Pa. To find the critical hydraulic gradient, simulations with bottom pressures, 7.84 Pa, 78.4 Pa, 3920.0 Pa and 7840.0 Pa, are respectively carried out. The corresponding hydraulic gradients, computed by Eq. 21, are 0.01, 0.1, 1.0, 5.0 and 10.0, respectively. It has been reported when the size ratio of particle diameter to lattice size is greater than 20, an accurate solution can be guaranteed. Hence, the grid size is selected as 0.001m, dividing the domain into 20×20×80 lattices, so that the diameter of the particle covers 20 lattices. The relaxation parameter τ is 0.5000005. Other parameters, such as density, kinematic viscosity of fluid and contact stiffness of solid, are given in Table 2.

$$i = \Delta P/h \tag{21}$$

Under the driving of upward fluid flow, the increasing hydrodynamic force gradually offsets downward resultant force of gravitational and buoyancy forces. The evolution of the acceleration

of top three particles under different hydraulic gradient is given in Fig. 9. Then, the corresponding accelerations at equilibrium state are shown in Fig. 10. Through computing the intersection, so-called critical hydraulic gradient at which the particle becomes fluidized, of X coordinate and the fitting curve, the critical hydraulic gradient obtained from numerical simulations is found to be 0.887. The analytical critical hydraulic gradient (Craig, 2013) can be determined by

$$i_{cr} = \frac{G_s - 1}{1 + e} \tag{22}$$

The specific gravity G_s of particles is 2.75 and the void ratio of the column packing is 1.099. Then, the analytical critical hydraulic gradient, marked in blue in Fig. 10, is calculated to be 0.834. It is found that the analytical vale and numerical results are very close.

To validate the bond model, the second model with hydraulic gradient of 5.0 is undertaken. In model 2, the top three moveable particles are pined together and they are not allowed to separate; at the meantime, the fixed bottom particle and adjacent particle are bonded together. The bond stiffness and strength are given in Table 2. Other parameters are the same as those in model 1. The hydrodynamic forces applied to three moveable spheres in both models are given in Fig11. Comparisons of corresponding accelerations can be seen in Fig. 12. The resultant force of gravitational and buoyancy forces of three moveable spheres is 0.2155 N. It is found that in the first model the acceleration becomes positive after 10000 time steps when the hydrodynamic force exceeds 0.2155 N. While in the second model with bond, the acceleration is around zero until the hydrodynamic force exceeds 0.2275 N, which is the sum of the resultant force and bond strength, after about 24000 time steps. Then, the bond breaks, and the acceleration becomes positive suddenly.

Table 2 Parameters for the solid and fluid

Parameter	Value	Parameter	Value
Particle density (kg/m^3)	2750	Fluid density (kg/m^3)	1000
Friction coefficient	0.3	kinematic viscosity (m^2/s)	1.0×10^{-6}
Particle contact stiffness (N/m)	5.0×10^{7}	Bond normal stiffness (N/m)	5.0×10^{5}
Bond strength (N)	0.012	Bond shear stiffness (N/m)	1.0×10^{5}

3.2 Erosion in granular particle-soil system

In the geotechnical engineering a granular filter is the typically well-graded sand or sandy gravel (Craig, 2013). It is an effective way to eliminate or alleviate this risk of seepage erosion occurring in dams and embankments, and it has been adopted in practice engineering for almost a hundred years. However, the behaviour of granular filters is still not well understood and the designing of granular filters are made according to the design criteria derived from experiments which are still the most important methods in the research of granular filters.

In this section, the applicability of the coupled bonded particle and lattice Boltzmann method will be demonstrated by modelling the performance of granular filters of different particle size distribution designed according to the design criteria.

3.2.1 Design criteria (Terzaghi and Peck, 1948, Zou et al., 2013, Huang et al., 2014)

In practice, the grain-size distribution of the filter should be properly manipulated to avoid the potential danger. Generally speaking, two conditions should be satisfied:

a) The size of the voids in the filter material should be small enough to hold the larger particles of the protected material in place. To be specific, the effective diameter $D_{15(F)}$ in the filter should be less than 4 × $D_{85(S)}$ of the protected soil.

$$R_1 = \frac{D_{15(F)}}{D_{85(S)}} \leq 4 \tag{23}$$

b) The filter material should have a high hydraulic conductivity to prevent build-up of large seepage forces and hydrostatic pressures in the filters. It means the effective pore diameter $D_{15(S)}$ is about 0.2* $D_{15(F)}$ to 0.25* $D_{15(F)}$ of the filter.

$$\frac{D_{15(F)}}{D_{15(S)}} \geq 5 \tag{24}$$

where $D_{15(F)}$ - diameter through which 15% of filter material will pass;

$D_{15(S)}$ - diameter through which 15% of soil to be protected will pass;

$D_{85(S)}$ - diameter through which 85% of soil to be protected will pass.

3.2.2 Numerical model

The base soil-filter system is modelled by a cubic sample (0.1m×0.1m×0.2m). The lateral boundaries are fixed walls, a stationary wall only effective for solid particles is exerted to support base soils and the granular filter, whilst, the upper surface of the granular filter is fixed. Apparently, the setup of soil-filter system (see Fig. 13) includes two parts: the base soil at the lower part and the filter layer.

The base soil, the so-called protected soil, is comprised of 1500 various-sized particles. The cohesive force is considered through the bond models. In order to demonstrate the feasibility and accuracy of the proposed method, three filters, with different size ratios R_1= 2.29, 3.43 and 4.29, are constructed. The particles size distribution curves of filters and protected soils are given in Fig. 14. Two of filters comply with the design criteria and the last filter disobeys it. During the whole simulation, a continuous hydraulic loading is applied at the bottom. It has been reported when the size ratio of particle diameter to lattice size is 20, an accurate solution can be

achieved in the first test case. In the simulation involving thousands of solid particles, especially for 3D problem, to increase the computing efficiency, the size ratio of particle diameter to lattice size cannot strictly satisfy as large as 20. In this example, to reduce the computing cost, the lattice space adopted is 1.0 mm, thus the problem domain is divided into 100×100×200 grids. The relaxation parameter τ is 0.5000005. The time step of LBM, determined by Eq. 11, is 1.667×10^{-5} s. Other model parameters are the same as those in the previous example except the critical bond strength of 10 N.

3.2.3 Results

During the whole simulation of the performance of granular filters, the transport of base soils and the evolution of hydraulic pressures can be successfully observed. The snapshots of the fluid-particle system with the representative ratio R1=3.43 at different instants are shown in Fig. 15. It is found that at the initial stage the soil particles will move upward under the driving of hydraulic loading. Once these particles start to penetrate into the filter large-sized particles will be blocked by the filter. Finally, only the small-sized particles can pass through the filter. Detailed transport of soil particles within this filter can be seen in Fig. 15.

From Fig. 16, it can be found that both fine and coarse particles of the protected soil pass through the large filter with R_1=4.29. While, only part of fine particles can flow out from the medium filter with R_1=3.43, and few soil particles penetrate into the small filter with R_1=2.29. To provide insight into the progress of soil erosion, a quantitative erosion ratio is introduced and it is defined as the percentage of the mass of eroded particles over the total mass of the base soil (see Eq. 25). The soil particles flow out of the granular filter are treated as eroded particles.

$$R_{erosion} = \frac{Mass_{erosion}}{Mass_{soil}} = \frac{\sum_{i=1}^{N_l} r_i^3}{\sum_{i=1}^{N} r_i^3} \tag{25}$$

where N_l and N are respectively the numbers of eroded particles and total number of the base soil. r_i is the radius of the particle under consideration.

Fig. 17 gives the evolution of erosion ratio with normalised time where $t=t/t_0-1$. t_0 is the initiation time of erosion. At the early stage of simulations soil particles transport at a low speed and no eroded particles can be detected. A certain time (t0) later, the erosion ratio of protected soils in large filter grows up rapidly; while, the speed of particle erosion in medium is much lower. The final erosion ratios for filters are 10.0% for the large filter, 0.5% for the medium filter and 0.001% for the small filter at the end, respectively. Thus, the medium and small filters, which comply with the design criteria, can effectively alleviate or eliminate the appearance of particle erosions.

It is noticed that to simulate the natural sand, small bond strength is applied to above filters. To evaluate the effect of bond on erosion ratio, another two simulations with critical bond strength 100 N and 1000 N are carried out for the large filter. The final erosion ratio for different bond strengths is shown in Fig. 18. With the increase of bond strength, some bonded particles, which undertake hydrodynamic forces smaller that the bond strength, become hard to break.

In the modelling of the transport of soil particles in granular filters, the movement and distribution of soil particles at any instants can be readily captured at the pore level. Three filters samples are prepared for tests, and the numerical results match the design criteria well. For detailed simulation accounting for the effect of hydraulic gradient and other factors can be seen in our previous work (Wang at al., 2017c). Compared to the continuum-based methods, this novel approach can provide a microscopic insight into the particle erosion process, thereby furthering the engineers' understanding of particle erosion problems in such fluid-particle systems.

It is found that the selection of fluid viscosity and relaxation parameter should be very careful when the fluid is water. If the fluid is oil in DEM-LBM/BPLBM coupling, the simulation is more robust. If the fluid is water, to obtain a stable simulation the relaxation parameter τ should be greater than and greatly approaching 0.5, because the kinematic viscosity of water is much smaller. At the meantime, to avoid a very small time step, kinematic viscosity should not be too small. Because the time step is proportional to kinematic viscosity.

4. Conclusions

This paper presents a 3D bonded particle and lattice Boltzmann method for resolving the fluid-solid coupling problems in geotechnical engineering. It can be treated as an extension of DEM-LBM where a bond model accounting for strain softening in normal contact are incorporated to investigate the influence of cementation between fine particles. In addition, a novel 3D algorithm of immersed moving boundary scheme was also proposed to resolve fluid-particle interaction. This mesoscopic/microscopic coupling method can process fluid-particle interactions at the grain-level which commonly ranges from hundreds of microns to several centimetres.

Numerical simulations of the quicksand case of a single column of spheres and the performance of granular filters have well demonstrated the feasibility and accuracy of the coupled BPLBM approach. It gains further insight into the fine particle erosion in dams. Besides, the instantaneous state of the migration of soil particles can be readily observed. However, this coupled technique with high resolution is computationally expensive. The simulation of each 3D granular filter takes about 2 days. Therefore, the parallelization of BPLBM becomes an essence for 3D large-scaled simulations.

References

Alejandro, J. C. C. 2008. Application of the Smoothed Particle Hydrodynamics model SPHysics to free-surface hydrodynamics. *PhD thesis, Universidade De Vigo*.

Chen, S., Chen, H., Martinez, D. O. & W. H. Matthaeus 1991. Lattice Boltzmann model for simulation of magnetohydrodynamics. *Phys. Rev. Lett.,* 67**,** 3776-3779.

Cook, B. K., Noble, D. R. & Williams, J. R. 2004. A direct simulation method for particle-fluid systems. *Engineering Computations,* 21**,** 151-168.

Craig, R. F. 2013. *Soil mechanics*, Springer.

Cui, X., Li, J., Chan, A. & Chapman, D. 2014. Coupled DEM–LBM simulation of internal fluidisation induced by a leaking pipe. *Powder Technology,* 254**,** 299-306.

Dash, S. M., Lee, T. S., Lim, T. T. & Huang, H. 2014. A flexible forcing three dimension IB–LBM scheme for flow past stationary and moving spheres. *Computers & Fluids,* 95**,** 159-170.

Delenne, J.-Y., El Youssoufi, M. S., Cherblanc, F. & Bénet, J.-C. 2004. Mechanical behaviour and failure of cohesive granular materials. *International Journal for Numerical and Analytical Methods in Geomechanics,* 28**,** 1577-1594.

Delenne, J.-Y., Mansouri, M., Radjaï, F., Youssoufi, M. S. E. & Seridi, A. 2011. Onset of Immersed Granular Avalanches by DEM-LBM Approach. . *In:* BONELLI, S., DASCALU, C. & NICOT, F. (eds.) *Advances in Bifurcation and Degradation in Geomaterials.* Springer Netherlands.

Di Felice, R. 1994. The voidage function for fluid-particle interaction systems. *International Journal of Multiphase Flow*, 20, 153-159.

Dupuis, A., Chatelain, P. & Koumoutsakos, P. 2008. An immersed boundary–lattice-Boltzmann method for the simulation of the flow past an impulsively started cylinder. *Journal of Computational Physics,* 227**,** 4486-4498.

El Shamy, U. 2004. A coupled continuum-discrete fluid–particle hydromechanical model for granular soil liquefaction. *Ph.D. thesis, Rensselaer Polytechnic Institute, Troy, NY*.

Feng, Y. T., Han, K. & Owen, D. R. J. 2007. Coupled lattice Boltzmann method and discrete element modelling of particle transport in turbulent fluid flows: Computational issues. *International Journal for Numerical Methods in Engineering,* 72**,** 1111-1134.

Feng, Y. T., Han, K. & Owen, D. R. J. 2010. Combined three-dimensional lattice Boltzmann method and discrete element method for modelling fluid-particle interactions with experimental assessment. *International Journal for Numerical Methods in Engineering,* 81**,** 229-245.

Feng, Y. T. & Owen, D. R. J. 2002. An augmented spatial digital tree algorithm for contact detection in computational mechanics. *International Journal for Numerical Methods in Engineering,* 55**,** 159-176.

Feng, Z. G. & Michaelides, E. E. 2004. The immersed boundary-lattice Boltzmann method for solving fluid-particles interaction problems. *Journal of Computational Physics,* 195**,** 602-28.

Filippova, O. & Hänel, D. 1998. Grid Refinement for Lattice-BGK Models. *Journal of Computational Physics,* 147**,** 219-228.

Goodarzi, M., Kwok, C. Y. & Tham, L. G. 2015. A continuum-discrete model using Darcy's law: formulation and verification. *International Journal for Numerical and Analytical Methods in Geomechanics,* 39**,** 327-342.

Guo, Z., Zheng, C. & Shi, B. 2002. Discrete lattice effects on the forcing term in the lattice Boltzmann method. *Physical Review E,* 65**,** 046308.

Hakuno, M. & Tarumi, Y. 1988. A granular assembly simulation for the seismic liquefaction of sand. *Structural Eng. / Earthquake Eng.,* 5**,** 333-342.

Han, Y. and Cundall, P. A. 2011. Resolution sensitivity of momentum-exchange and immersed boundary methods for solid–fluid interaction in the lattice Boltzmann method. *Int. J. Numer. Meth. Fluids*, 67: 314–327.

Han, Y. & Cundall, P. A. 2013. LBM–DEM modeling of fluid–solid interaction in porous media. *Int. J. Numer. Anal. Meth. Geomech.*, 37: 1391–1407.

Hu HH. 1996. Direct simulation of flows of solid–liquid mixtures. *International Journal of Multiphase Flow*; 22:335–352.

Huang, Q.-F., Zhan, M.-L., Sheng, J.-C., Luo, Y.-L. & Su, B.-Y. 2014. Investigation of fluid flow-induced particle migration in granular filters using a DEM-CFD method. *Journal of Hydrodynamics, Ser. B,* 26**,** 406-415.

Itasca Consulting Group Inc 2002. Particle Flow Code in 2 Dimensions. *version 3.0. Minnesota, U.S.A.*

Jiang, M. J., Sun, Y. G., Li, L. Q. & Zhu, H. H. 2012. Contact behavior of idealized granules bonded in two different interparticle distances: An experimental investigation. *Mechanics of Materials,* 55.

Jiang, M. J., Yu, H. S. & Harris, D. 2006. Bond rolling resistance and its effect on yielding of bonded granulates by DEM analyses. *International Journal for Numerical and Analytical Methods in Geomechanics,* 30**,** 723-761.

Jing, L., Kwok, C.Y., Leung, A.Y.F. & Sobral, Y. 2015. Extended CFD-DEM for free-surface flow with multi-size granules. *International Journal of Numerical and Analytical Methods in Geomechanics*. 40: 62-79.

Kafui, K. D., Thornton, C. & Adams, M. J. 2002. Discrete particle-continuum fluid modelling of gas–solid fluidised beds. *Chemical Engineering Science*, 57, 2395-2410.

Kao, P. H. & Yang, R. J. 2008. An investigation into curved and moving boundary treatments in the lattice Boltzmann method. *Journal of Computational Physics,* 227**,** 5671-5690.

Kazerani, T., Zhao, G.F. & Zhao, J. 2010. Dynamic Fracturing Simulation of Brittle Material using the Distinct Lattice Spring Method with a Full Rate-Dependent Cohesive Law. *J. Rock Mech Rock Eng*, 43: 717-726.

Ladd, A. J. C. 1994. Numerical simulations of particulate suspensions via a discretized Boltzmann equation. Part 1. Theoretical foundation. *Journal of Fluid Mechanics,* 271**,** 285-309.

Ladd, A. J. C. & Verberg, R. 2001. Lattice-Boltzmann Simulations of Particle-Fluid Suspensions. *Journal of Statistical Physics,* 104**,** 1191-1251.

Lallemand, P. & Luo, L.-S. 2003. Lattice Boltzmann method for moving boundaries. *Journal of Computational Physics,* 184**,** 406-421.

Leonardi, A., Wittel, F. K., Mendoza, M., Vetter, R., & Herrmann, H. J. 2016. Particle–Fluid–Structure Interaction for Debris Flow Impact on Flexible Barriers. *Computer–Aided Civil and Infrastructure Engineering*, 31**,** 323-333.

Li, X., Zienkiewicz, O. C. & Xie, Y. M. 1990. A numerical model for immiscible two-phase fluid flow in a porous medium and its time domain solution. *International Journal for Numerical Methods in Engineering,* 30**,** 1195-1212.

Lominé, F., Scholtès, L., Sibille, L. & Poullain, P. 2013. Modeling of fluid–solid interaction in granular media with coupled lattice Boltzmann/discrete element methods: application to piping erosion. *International Journal for Numerical and Analytical Methods in Geomechanics,* 37**,** 577-596.

Mansouri, M., Delenne, J. Y., El Youssoufi, M. S. & Seridi, A. 2009. A 3D DEM-LBM approach for the assessment of the quick condition for sands. *Comptes Rendus Mécanique,* 337**,** 675-681.

Mei, R., Luo, L.-S. & Shyy, W. 1999. An Accurate Curved Boundary Treatment in the Lattice Boltzmann Method. *Journal of Computational Physics,* 155**,** 307-330.

Mei, R., Yu, D., Shyy, W. & Luo, L.-S. 2002. Force evaluation in the lattice Boltzmann method involving curved geometry. *Physical Review E,* 65**,** 041203.

Mohamad, A. A. & Kuzmin, A. 2010. A critical evaluation of force term in lattice Boltzmann method, natural convection problem. *International Journal of Heat and Mass Transfer,* 53**,** 990-996.

Munjiza, A. 2004. The Combined Finite-Discrete Element Method. London.

Noble, D. R. & Torczynski, J. R. 1998. A Lattice-Boltzmann Method for Partially Saturated Computational Cells. *International Journal of Modern Physics C,* 09**,** 1189-1201.

Owen, D. R. J., Leonardi, C. R. & Feng, Y. T. 2011. An efficient framework for fluid–structure interaction using the lattice Boltzmann method and immersed moving boundaries. *International Journal for Numerical Methods in Engineering,* 87**,** 66-95.

Peng, Y., Shu, C., Chew, Y. T., Niu, X. D. & Lu, X. Y. 2006. Application of multi-block approach in the immersed boundary–lattice Boltzmann method for viscous fluid flows. *Journal of Computational Physics,* 218**,** 460-478.

Potyondy, D. O. 2007. Simulating stress corrosion with a bonded-particle model for rock. *International Journal of Rock Mechanics and Mining Sciences,* 44**,** 677-691.

Potyondy, D. O. & Cundall, P. A. 2004. A bonded-particle model for rock. *International Journal of Rock Mechanics and Mining Sciences,* 41**,** 1329-1364.

Obermayr, M., Dressler, K., Vrettos, C. & Eberhard, P. 2013. A bonded-particle model for cemented sand. *Computers and Geotechnics*, 49, 299-313.
Shu, C., Liu, N. & Chew, Y. T. 2007. A novel immersed boundary velocity correction–lattice Boltzmann method and its application to simulate flow past a circular cylinder. *Journal of Computational Physics,* 226**,** 1607-1622.
Strack, O. E. & Cook, B. K. 2007. Three-dimensional immersed boundary conditions for moving solids in the lattice-Boltzmann method. *International Journal for Numerical Methods in Fluids,* 55**,** 103-125.
Terzaghi, K. & Peck, R. B. 1948. *Soil Mechanics in Engineering Practice,* New York, Wiley.
Thornton, C. & Yin, K. K. 1991. Impact of elastic spheres with and without adhesion. *Powder Technology,* 65**,** 153-166.
Tsuji, Y., Tanaka, T. & Ishida, T. 1992. Lagrangian numerical simulation of plug flow of cohesionless particles in a horizontal pipe. *Powder Technology*, 71, 239-250.
Vu-Quoc, L., Lesburg, L. & Zhang, X. 2004. An accurate tangential force–displacement model for granular-flow simulations: Contacting spheres with plastic deformation, force-driven formulation. *Journal of Computational Physics,* 196**,** 298-326.
Wang, M. 2016. *A Coupled Bonded Particle and Lattice Boltzmann Method with its Application to Geomechanics.* PhD, Swansea University, UK.
Wang, M., Feng, Y. T. & Wang, C. Y. 2016. Coupled bonded particle and lattice Boltzmann method for modelling fluid–solid interaction. *International Journal for Numerical and Analytical Methods in Geomechanics***,** 40**,** 1383-1401.
Wang, M., Feng, Y. T. & Wang, C. Y. 2017a. Numerical investigation of initiation and propagation of hydraulic fracture using the coupled Bonded Particle–Lattice Boltzmann Method. *Computers & Structures***,** 181**,** 32-40.
Wang, M., Feng, Y. T., Wang Y. & Zhao T. T. 2017b. Periodic boundary conditions of discrete element method-lattice Boltzmann method for fluid-particle coupling. *Granular Matter*, 2017, 19(3), 43.
Wang, M., Feng, Y. T., Pande, G. N., Chan, A.H.C. & Zuo, W.X. 2017c. Numerical modelling of fluid-induced soil erosion in granular filters using a coupled bonded particle lattice Boltzmann method, *Computers and Geotechnics*, 82: 134-143.
Wu, C.-Y. & Guo, Y. 2012. Numerical modelling of suction filling using DEM/CFD. *Chemical Engineering Science,* 73**,** 231-238.
Wu, J. & Shu, C. 2009. Implicit velocity correction-based immersed boundary-lattice Boltzmann method and its applications. *Journal of Computational Physics,* 228**,** 1963-1979.
Wu, J. & Shu, C. 2010. Particulate flow simulation via a boundary condition-enforced immersed boundary-lattice Boltzmann scheme. *Communications in Computational Physics,* 7**,** 793.
Yu, D., Mei, R. & Shyy, W. 2003. A unified boundary treatment in lattice Boltzmann method. *New York: AIAA,* 953**,** 2003.
Zhang, J., Fan, L.-S., Zhu, C., Pfeffer, R. & Qi, D. 1999. Dynamic behavior of collision of elastic spheres in viscous fluids. *Powder Technology,* 106**,** 98-109.
Zhao, J. D. & Shan, T. 2013. Coupled CFD–DEM simulation of fluid–particle interaction in geomechanics, *Powder Technology*, 239: 248-258.
Zhao, T., Dai, F. & Xu, N., 2017. Coupled DEM-CFD investigation on the formation of landslide dams in narrow rivers, Landslides 14: 189-201
Zhu, H. P., Zhou, Z. Y., Yang, R. Y. & Yu, A. B. 2008. Discrete particle simulation of particulate systems: A review of major applications and findings. *Chemical Engineering Science,* 63**,** 5728-5770.
Zienkiewicz, O. C., Chan, A. H. C., Pastor, M., Schrefler, B. A. & Shiomi, T. 1999. Computational Geomechanics with special reference to Earthquake Engineering. *John Wiley and Sons Ltd, Chichester*.
Zou, Q.S. and He, X.Y. 1997. On Pressure and Velocity Boundary Condition for the Lattice Boltzmann BGK Model. *Physics of Fluids*, 9, 1591-1598.
Zou, Y.-H., Chen, Q., Chen, X.-Q. & Cui, P. 2013. Discrete numerical modeling of particle transport in granular filters. *Computers and Geotechnics,* 47**,** 48-56.

Figures

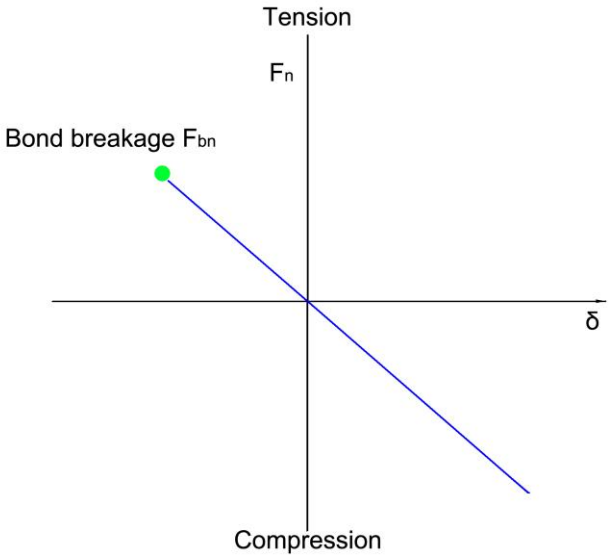

Fig. 1 Contact bond model: normal component

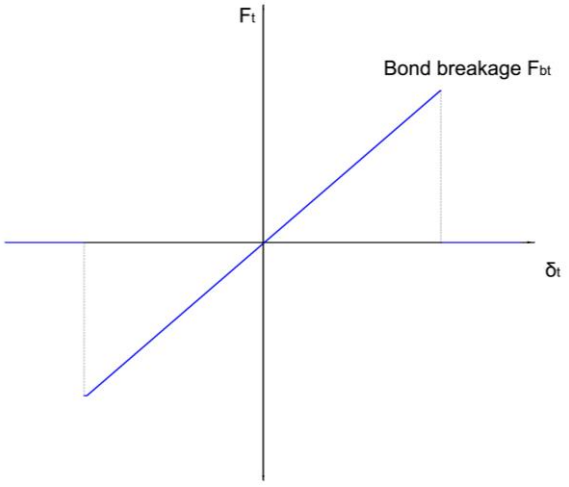

Fig. 2 Contact bond model: tangential component

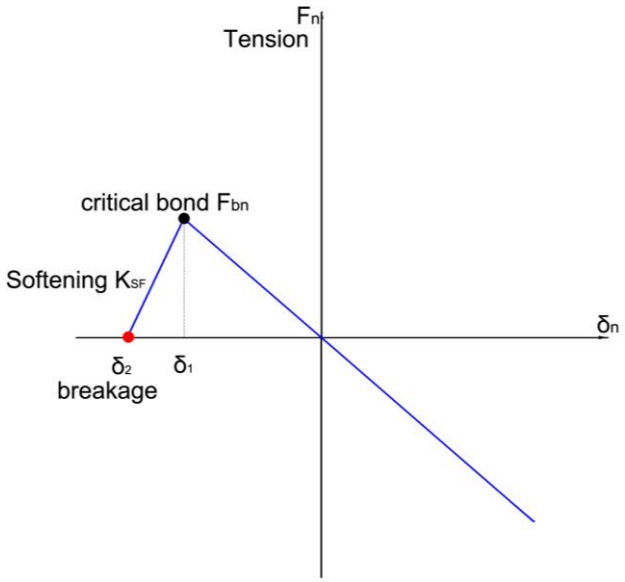

a. Normal bond model with strain softening

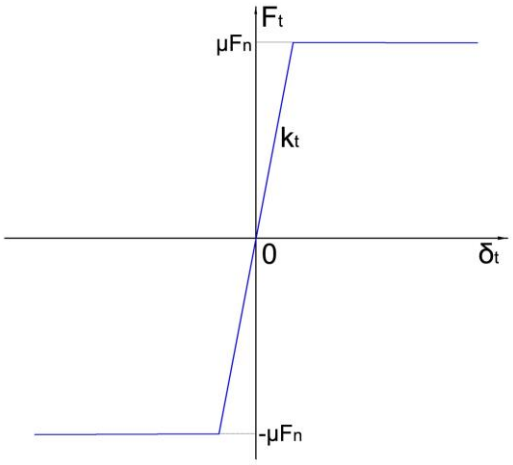

b. History dependent Coulomb friction model

Fig. 3 Advanced bond model

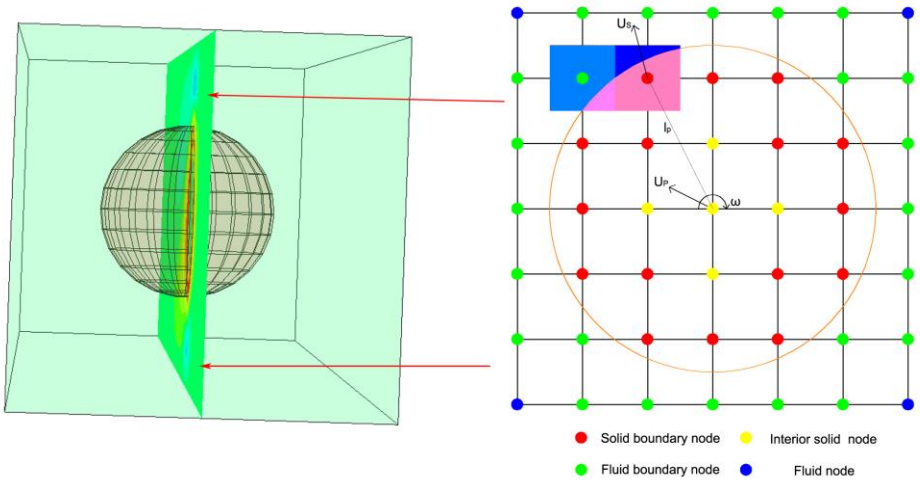

Fig. 4 IMB scheme

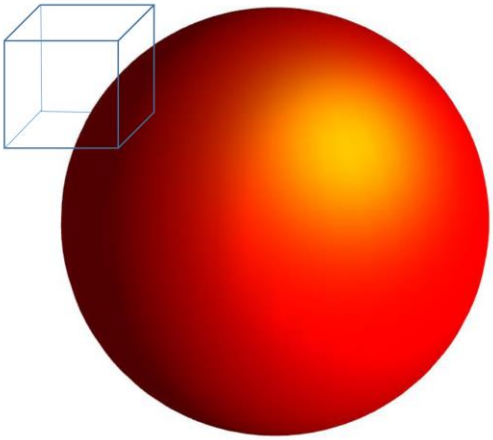

Fig. 5 Solid volumetric fraction in each nodal volume

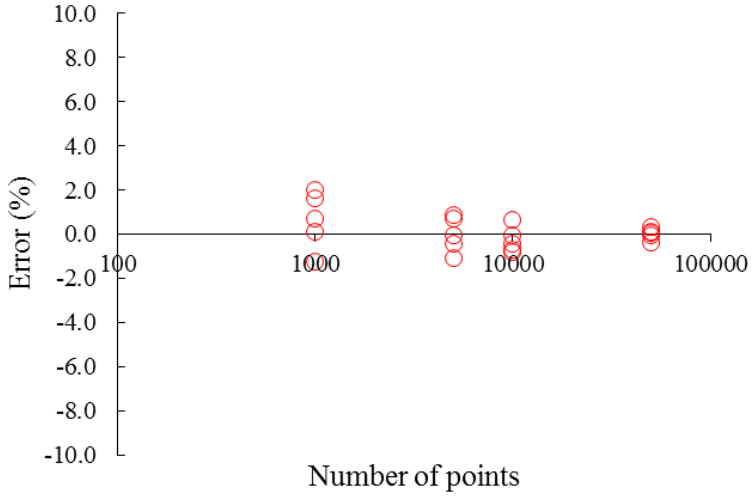

Fig. 6 Analysis error of Monte Carlo method

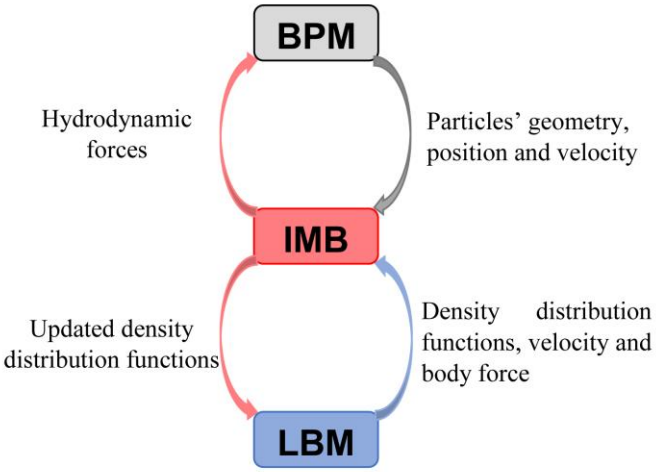

Fig. 7 BPM-LBM coupling procedure

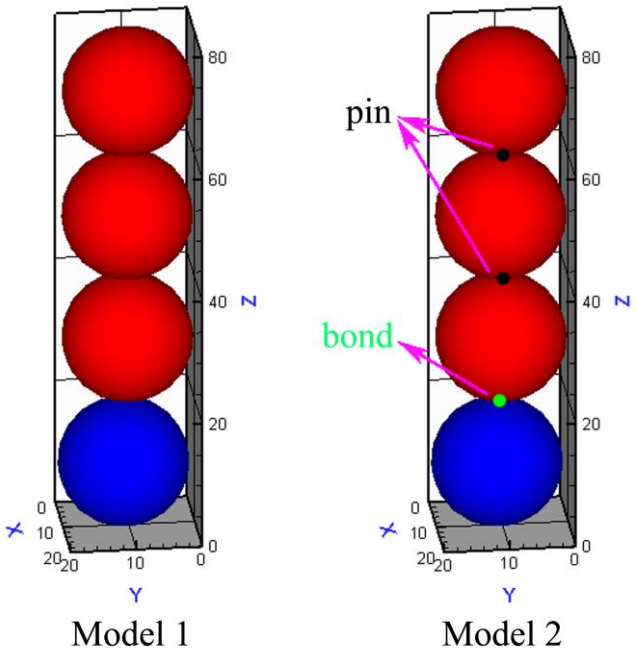

Fig. 8 Numerical model of quicksand

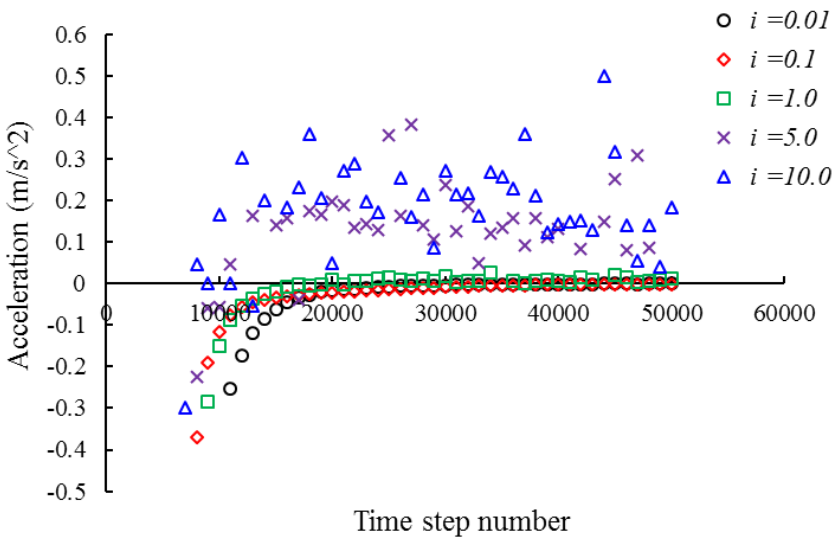

Fig. 9 Evolution of the acceleration under different hydraulic gradient

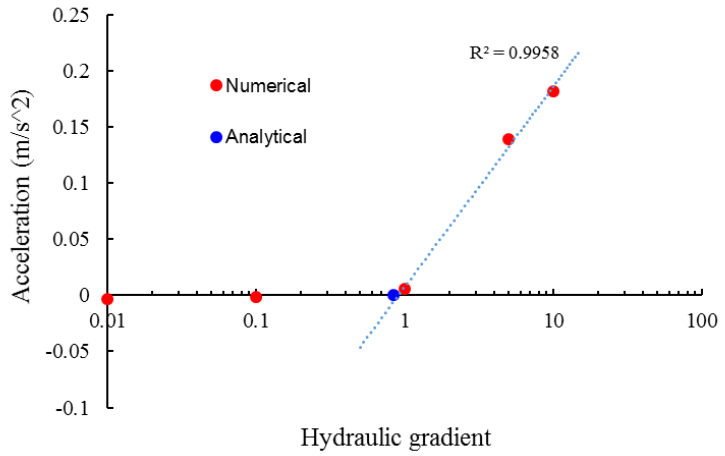

Fig. 10 Accelerations at equilibrium state under different hydraulic gradient

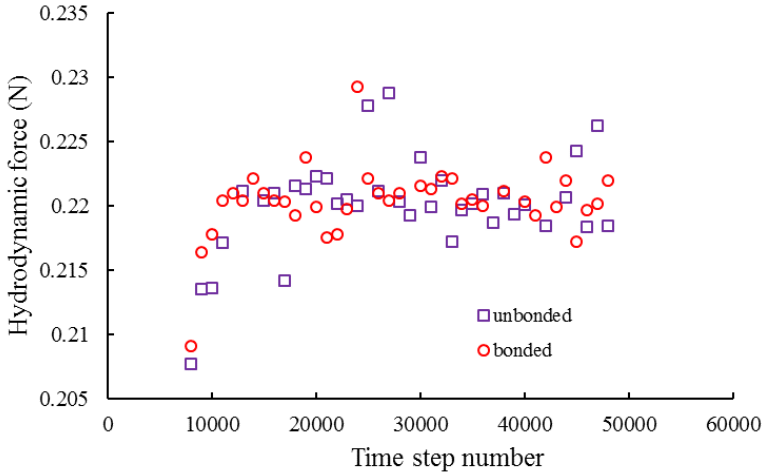

Fig. 11 Evolution of hydrodynamic forces

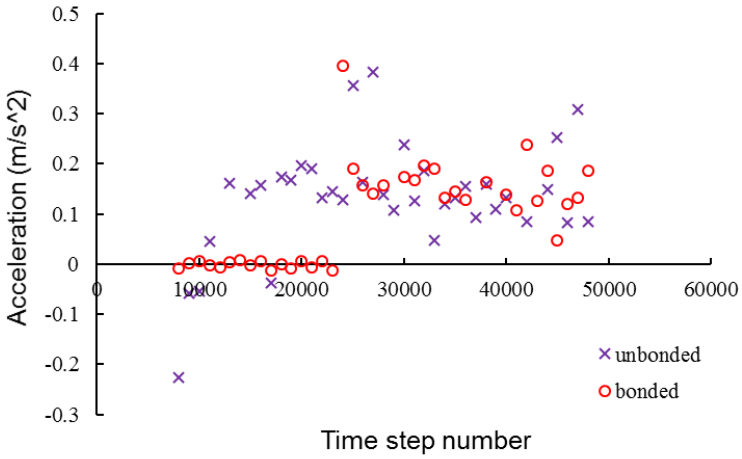

Fig. 12 Evolution of the acceleration

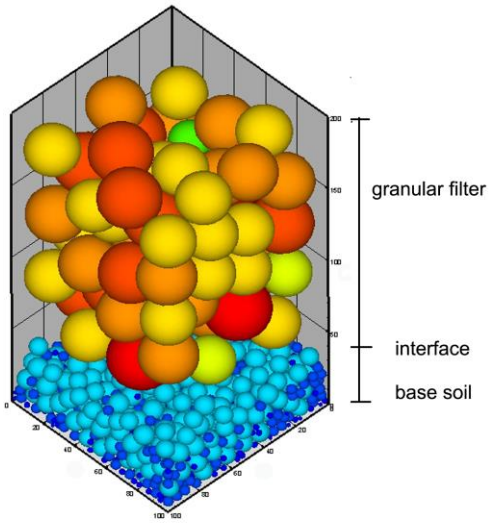

Fig. 13 Setup of a soil-filter system

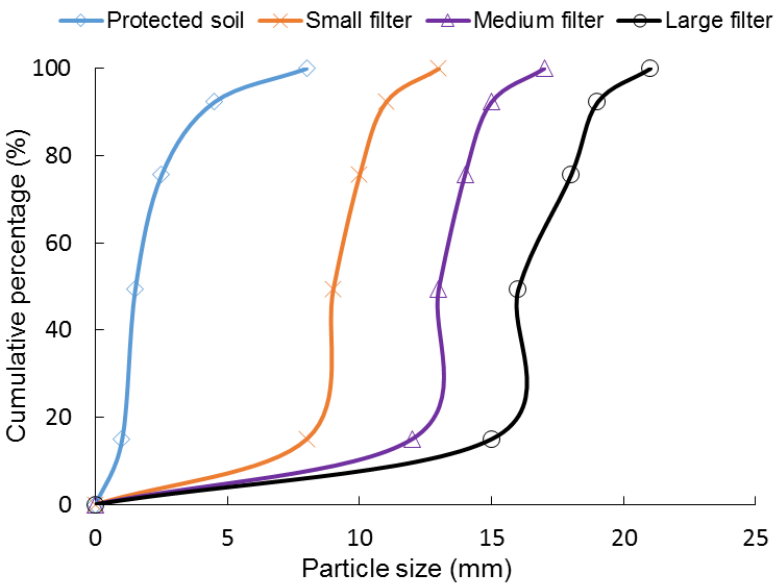

Fig. 14 Particles size distribution curves

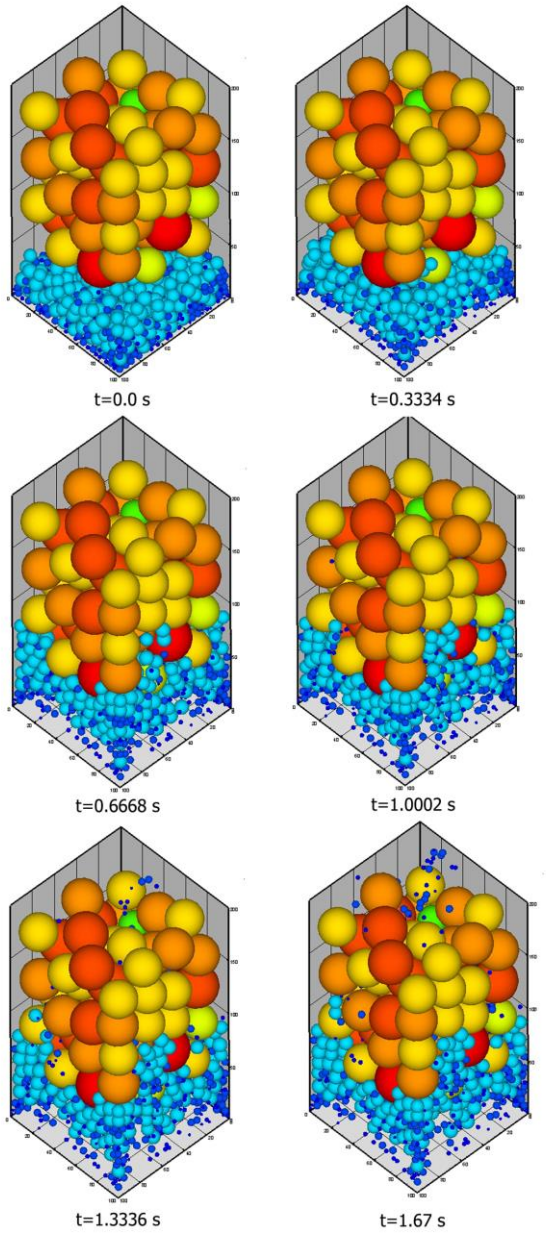

Fig. 15 Snapshots of the performance of medium filter (R_1=3.43)

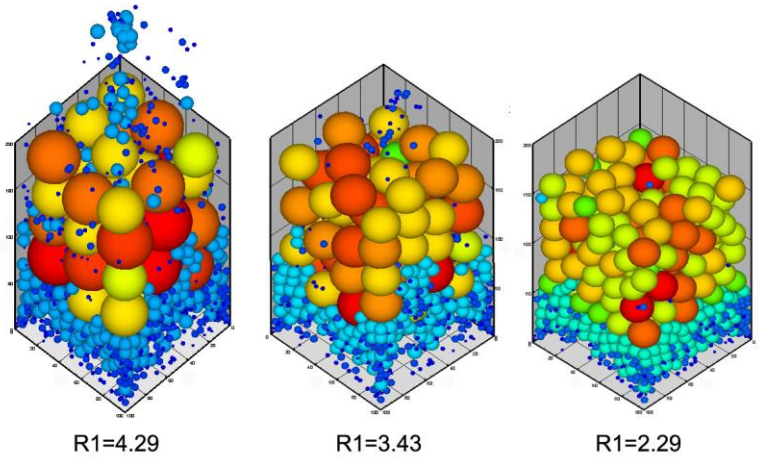

Fig. 16 Final distribution of soil particles in three filters

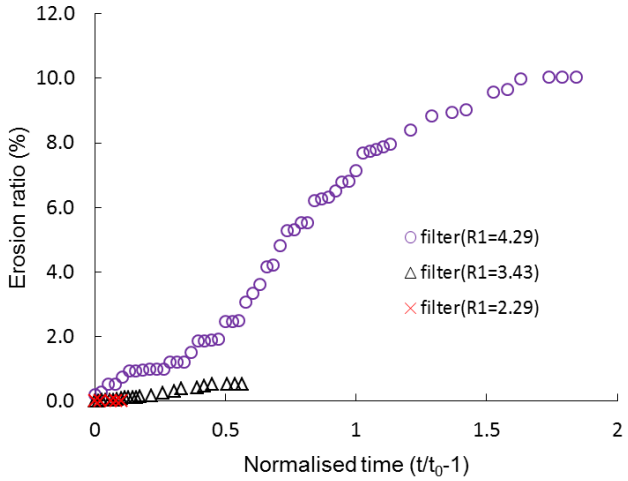

Fig. 17 Variation of erosion ratio in three filters

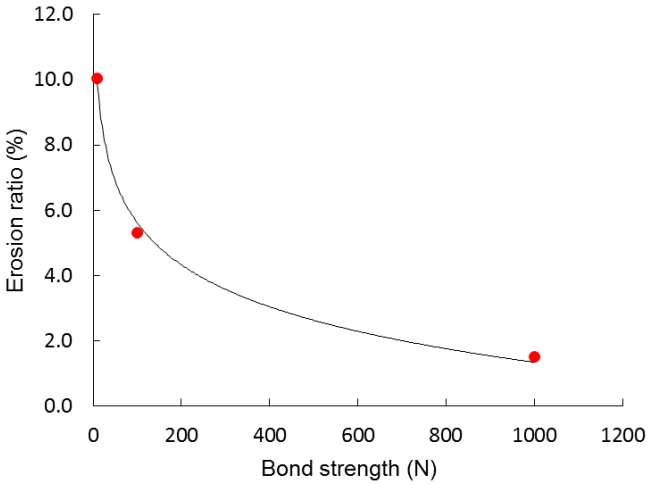

Fig. 18 Final erosion ratio versus critical bond strength in the large filter